

Finite transverse conductance in topological insulators under an applied in-plane magnetic field

Abhiram Soori ^{1,*} and Dhavala Suri ²

¹*School of Physics, University of Hyderabad, C. R. Rao Road, Gachibowli, Hyderabad-500046, India*

²*Centre for Interdisciplinary Sciences, Tata Institute of Fundamental Research, Hyderabad-500046, India*

Recently, in topological insulators (TIs) the phenomenon of planar Hall effect (PHE) wherein a current driven in presence an in-plane magnetic field generates a transverse voltage has been experimentally witnessed. There have been a couple of theoretical explanations that explain the origin of this phenomenon. We suggest an origin of this effect based on scattering theory on a normal metal-TI-normal metal junction and calculate the conductances in longitudinal and transverse directions to the applied bias. The transverse conductance depends on the location and is zero in the drain electrode when the chemical potentials on the top and the bottom surfaces of the TI are equal. The longitudinal conductance is π -periodic in ϕ -the angle between the bias direction and the direction of the in-plane magnetic field. The transverse conductance is π -periodic in ϕ when the chemical potentials of the top and the bottom TI surfaces are the same whereas it is 2π -periodic in ϕ when the chemical potentials of the top and the bottom surfaces are different. As a function of the magnetic field, the magnitude of transverse conductance increases initially, peaks. At higher magnetic fields, it decays for angles ϕ closer to $0, \pi$ whereas oscillates for angles ϕ close to $\pi/2$. We understand the features in the obtained results, which agree with the existing experimental results.

I. INTRODUCTION

In the last few decades, novel materials such as topological insulators (TIs) and Weyl semimetals which exhibit nontrivial electrical properties stemming from the topology of their bandstructures were invented¹⁻⁴. In Weyl semimetals, a nonzero transverse voltage appears in response to current in presence of an external magnetic field⁵⁻⁷. The transverse voltage lies in the same plane as current and applied magnetic field and this phenomenon is called planar Hall effect (PHE). PHE along with negative longitudinal magnetoresistance has been seen as a direct signature of chiral anomaly in Weyl semimetals. PHE has also been observed in TIs⁸⁻¹⁰ and its origin is ascribed to spin-flip scattering of surface electrons from impurities. Another explanation of PHE comes from the tilting of the Dirac cone that describes the surface states of the TIs¹¹. Also there has been an attempt at explaining PHE emanating from the bulk states of the TI¹². It is interesting to note that PHE in TIs was predicted by considering scattering at junction of TIs with a ferromagnet in proximity to one part of the TI surface¹³, without the need of either the scattering from impurities or the titling of the Dirac cones due to magnetic field. But a TI has two surfaces- one on top and another at bottom, as a result, it is not clear whether the transverse deflections of the incident electrons will cancel from the two surfaces. Motivated by these developments, we examine transport in a system of in-plane magnetic field applied to top and bottom surfaces of a TI connected to two-dimensional normal metal (NM) leads on either sides. We follow Lanaduer-Büttiker approach¹⁴⁻¹⁶ and calculate currents in transverse and longitudinal directions in response to a bias applied in the longitudinal direction. This is in contrast to the experiments where a current is driven in longitudinal direction and voltages developed

in transverse and longitudinal directions are measured in Hall bar geometry. Finally, we study the effect of unequal chemical potentials on the top and the bottom surfaces of TI which can be achieved in experiments by applying different gate voltages to the two surfaces.

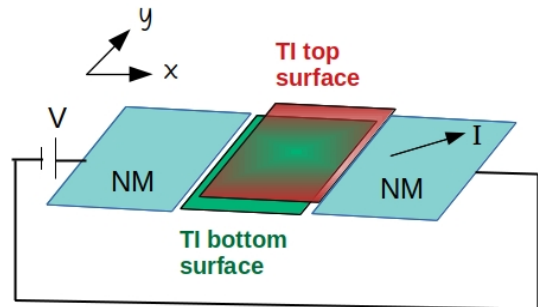


FIG. 1. Schematic diagram of the setup: the topological insulator (TI) is connected to normal metal (NM) leads on either sides. The two NM's and the TI are taken to be infinitely long along y . Both the NM leads are semi-infinite along x . A voltage V applied from left NM to the right NM results in a current I . Planar Hall effect is when the current I has a nonzero component along y direction. Such a transverse current could be either in the TI region or in the right NM region.

The paper is organized as follows. In sec. II, the system under consideration and details of the calculation comprising of the Hamiltonian, the boundary conditions and the formulae for the longitudinal and the transverse conductances are discussed. In sec. III, the results are presented and analyzed. In sec. IV, we discuss the implications of our results and conclude.

II. DETAILS OF CALCULATION

The setup under study is a NM-TI-NM junction, with the TI in the middle having a top surface and a bottom surface as shown in the Fig. 1. Both the NMs and the TI are infinitely long along y . The NM lead on the left extends all the way from $x = -\infty$ to $x = 0$ and makes a

$$\begin{aligned}
 H &= \left[-\frac{\hbar^2}{2m} \left(\frac{\partial^2}{\partial x^2} + \frac{\partial^2}{\partial y^2} \right) - \mu_N \right] \sigma_0, \quad \text{for } x < 0 \text{ and } x > L, \\
 &= i\hbar v_F \left(\sigma_y \frac{\partial}{\partial x_t} - \sigma_x \frac{\partial}{\partial y_t} \right) + (b_x \cdot \sigma_x + b_y \cdot \sigma_y) - \mu_t \sigma_0, \quad \text{for } 0 < x_t < L, \\
 &= -i\hbar v_F \left(\sigma_y \frac{\partial}{\partial x_b} - \sigma_x \frac{\partial}{\partial y_b} \right) + (b_x \cdot \sigma_x + b_y \cdot \sigma_y) - \mu_b \sigma_0, \quad \text{for } 0 < x_b < L.
 \end{aligned} \tag{1}$$

Here, μ_N is the chemical potential of the NM leads, $\mu_{t/b}$ is the chemical potential on the top/bottom surface of the TI which can be controlled by an applied gate voltage, $(b_x, b_y) = b(\cos \phi, \sin \phi)$ where ϕ is the angle the in-plane magnetic field makes with x -axis (we refer to the Zeeman energy b as magnetic field), σ_0 is identity matrix and $\sigma_{x,y}$ are Pauli spin matrices. The in-plane magnetic field shifts the Dirac point of the top (bottom) surface to $\vec{k} = \pm(b_y, -b_x)/\hbar v_F$ respectively. The dispersion relations for the top and the bottom surfaces are respectively

$$E = -\mu_t \pm \sqrt{(\hbar v_F k_x - b_y)^2 + (\hbar v_F k_y + b_x)^2}, \tag{2}$$

$$E = -\mu_b \pm \sqrt{(\hbar v_F k_x + b_y)^2 + (\hbar v_F k_y - b_x)^2}, \tag{3}$$

where $k^2 = k_x^2 + k_y^2$.

To solve the scattering problem, boundary conditions need to be specified at $x = 0$ and $x = L$. Boundary conditions at NM-TI junctions have been discussed in literature¹⁷⁻¹⁹. The probability current operators for the top and bottom surfaces can be shown to be $\vec{j}_t = (-v_F \sigma_y, v_F \sigma_x)$ and $\vec{j}_b = (v_F \sigma_y, -v_F \sigma_x)$ respectively. So, the conservation of current along x -direction between NM and TI surfaces reads

$$\frac{\hbar \text{Im}[\psi_N^\dagger \partial_x \psi_N]_{x=x_0}}{mv_F} = -\psi_t^\dagger \sigma_y \psi_t|_{x_t=x_0} + \psi_b^\dagger \sigma_y \psi_b|_{x_b=x_0}, \tag{4}$$

at both the junctions located at $x_0 = 0, L$, where ψ_N is the wavefunction on the NM side and $\psi_{t/b}$ is the wavefunction on the top/bottom surface of the TI. This leads to the boundary conditions

$$\begin{aligned}
 \psi_N &= c[M(\chi_t)\psi_t + M(\chi_b)\psi_b], \\
 \frac{\hbar}{mv_F} \partial_x \psi_N - \chi_N \psi_N &= \frac{i}{c} \sigma_y \cdot \left[-M(\chi_t)\psi_t + M(\chi_b)\psi_b \right],
 \end{aligned} \tag{5}$$

junction with both the surfaces of TI along $x = 0$. TI extends from $x = 0$ to $x = L$ and makes a junction with the NM on the right along the line $x = L$. From now on, we shall denote the coordinates of the top (bottom) surface of the TI with a subscript t (b). The in-plane magnetic field applied is present only in the TI region. The NM lead on the right extends from $x = L$ to $x = \infty$. The Hamiltonian describing the system being investigated is

where all the wavefunctions and $\partial_x \psi_N$ are evaluated at each of the two junctions located at $x_0 = 0$ and $x_0 = L$. Here, $M(\chi) = \exp[i\chi\sigma_y]$ and the dimensionless parameters χ_N, χ_t and χ_b quantify the strengths of the delta-function barriers infinitesimally close to the junction from the NM-, top TI- and bottom TI- sides respectively^{17,20}. We shall set these parameters to zero at both the junctions to allow maximal transmission. We shall set $c = (mv_F/\sqrt{2m\mu_N})^{1/2}$ so that transmission of normally incident electron at the junction is perfect at zero energy in absence of a magnetic field¹⁹.

Due to translational invariance of the system in y -direction, the momentum $\hbar k_y$ along y can be taken to be equal in all the four regions. The wavefunction of a spin- σ electron incident from the left NM with energy E , making an angle θ with x -axis has the following form in different regions (except for a multiplicative factor of $e^{ik_y y}$):

$$\begin{aligned}
 \psi_N(x) &= (e^{ik_x x} + r_{\sigma,\sigma} e^{-ik_x x})|\sigma\rangle + r_{\bar{\sigma},\sigma} e^{-ik_x x}|\bar{\sigma}\rangle, \\
 &\quad \text{for } x < 0, \\
 \psi_p(x_p) &= s_{\sigma,p,+} e^{ik_{x,p,+} x_p} |k_{p,+}\rangle + s_{\sigma,p,-} e^{ik_{x,p,-} x_p} |k_{p,-}\rangle, \\
 &\quad \text{for } 0 < x_p < L, \text{ and } p = t, b, \\
 \psi_N(x) &= t_{\uparrow,\sigma} e^{ik_x x} |\uparrow\rangle + t_{\downarrow,\sigma} e^{ik_x x} |\downarrow\rangle, \text{ for } x > L,
 \end{aligned} \tag{6}$$

where $\sigma = \uparrow, \downarrow$, $\bar{\sigma}$ is the spin opposite to σ , $|\uparrow\rangle = [1, 0]^T$, $|\downarrow\rangle = [0, 1]^T$, $k_x = \sqrt{2m(\mu_N + E)} \cos \theta/\hbar$, $k_y = \sqrt{2m(\mu_N + E)} \sin \theta/\hbar$, $k_{x,p,s}$'s for $s = +, -$ correspond to the two roots for x -wavenumber obtained from the dispersion in the p -TI surface ($p = t, b$ stand for top, bottom surfaces) as a function of E and k_y , $|k_{p,s}\rangle$ is the spinor on p -TI surface for electron with wavenumber $(k_{x,p,s}, k_y)$ which can be found from the Hamiltonian for the TI and the coefficients $r_{\sigma',\sigma}$, $s_{\sigma,p,s}$, $t_{\sigma',\sigma}$ are to be determined by matching the boundary conditions in eq. (5) at $x_0 = 0, L$.

The component of the current along x is conserved and is same anywhere. But along y , k_y is same in any

region and the component of current along y need not be same. If $\psi_{p,\sigma}(x)$ is the wavefunction due to an σ -spin electron incident at an angle θ at energy E on p -TI surface at $x_p = x$ in the range $0 \leq x_p \leq L$, the current along y at the location x from this wavefunction will be $I_{\sigma,y}(E, \theta)(x) = ev_F \sum_{p=t,b} \psi_{p,\sigma}(x)^\dagger \sigma_p \sigma_x \psi_{p,\sigma}(x)$, where e is electron charge, $\sigma_t = 1$ and $\sigma_b = -1$. If $[I_x, I_y(x)]$ is the current flowing at x in response to a voltage bias V in the bias window $(0, eV)$, the longitudinal and transverse differential conductances are defined as $G_{xx} = dI_x/dV$ and $G_{yx}(x) = dI_y(x)/dV$. These are given by the expressions

$$G_{xx} = \frac{\sqrt{2m(\mu_N + eV)}}{mv_F} G_0 \sum_{\sigma,\sigma'=\uparrow,\downarrow} \int_{-\pi/2}^{\pi/2} d\theta \cos \theta |t_{\sigma',\sigma}|^2,$$

$$G_{yx}(x) = \frac{G_0}{ev_F} \sum_{\sigma=\uparrow,\downarrow} \int_{-\pi/2}^{\pi/2} I_{\sigma,y}(eV, \theta, x) d\theta, \quad (7)$$

where $G_0 = (e^2/h) \cdot (mv_F L_y/h)$ and L_y is the length of the system in y -direction. The current deflected in the transverse direction in the right NM is same at all locations $x > L$ and the transverse differential conductance due to this current is given by

$$G_{yx}(x > L) = \frac{\sqrt{2m(\mu_N + eV)}}{mv_F} G_0 \sum_{\sigma,\sigma'=\uparrow,\downarrow} \int_{-\pi/2}^{\pi/2} d\theta \sin \theta |t_{\sigma',\sigma}|^2 \quad (8)$$

III. RESULTS AND ANALYSIS

To obtain numerical results, we shall fix μ_N and v_F , and choose other parameters as combinations of these parameters. The mass m decides the size of the Fermi wavenumber. We choose $m = 0.025\mu_N/v_F^2$ so that the wavenumbers on NM and TI at energy $-0.2\mu_N$ are equal when $\mu_t = \mu_b = 0$ and $b = 0$. The length of the TI is chosen to be $L = 5\hbar v_F/\mu_N$. These are the values of the parameters unless otherwise stated.

A. $\mu_t = \mu_b$

First, we set $\mu_t = \mu_b = 0.1\mu_N$ and study the dependence of G_{xx} and $G_{yx}(L/2)$ on the bias at different angles ϕ when the magnitude of the magnetic field is fixed at $b = 0.4\mu_N$ in Fig 2(a) and Fig. 2(b) respectively. The slow increase in G_{xx} with bias is due to the increase in density of states of incident electrons. For an angle ϕ between x -axis and the magnetic field, the Dirac cones on the TI surfaces are displaced in y -direction by an amount $|b \cos \phi/(\hbar v_F)|$ thereby making the wavenumbers $k_{x,p,s}$'s in the TI region complex (when $\cos \phi \neq 0$) for a range of angle of incidence θ . This reduces the transmission probabilities $|t_{\sigma,\sigma'}|^2$ for larger values of $|\cos \phi|$ and for larger values of $|b|$ which agrees with the observed features of

G_{xx} in Fig. 2(a,c). In Fig. 2(b,d), we find that $G_{yx}(L/2)$ is exactly zero at $\phi = 0, \pm\pi/2, \pi$. When $\phi = \pm\pi/2$, the Dirac cone is shifted along x -direction and the system is symmetric under $y \rightarrow -y$ thereby giving zero total current along y . When $\phi = 0, \pi$, the Dirac cones in the top and bottom surfaces are displaced exactly along $\pm y$ directions, and the currents deflected along y from the top and the bottom surfaces are equal in magnitude and opposite in sign thus giving zero G_{yx} . Now, we address the question why there is a nonzero $G_{yx}(L/2)$ for a nonzero b in a direction ϕ other than $0, \pm\pi/2, \pi$. Under a magnetic field (b_x, b_y) , the Dirac points of the top and the bottom surfaces are shifted to $\pm(b_y, -b_x)/(\hbar v_F)$. The currents in y -direction carried by the electrons incident at angles θ and $-\theta$ on one surface do not cancel due to a finite shift of the Dirac cone in y -direction. At the same time, the net current in y -direction carried by the top surface and the bottom surface do not cancel despite the opposite shifts of the two Dirac cones because the wavenumbers in x -direction of the corresponding surfaces $k_{x,t,s}$ and $k_{x,b,s}$ are different. From Fig. 2(b), it can be seen that at $eV = -\mu_t = -\mu_b$, the transverse conductance is exactly zero implying that the net current in the transverse direction carried by the evanescent waves in the TI region is zero. The transverse conductance $G_{yx}(x)$ is π -periodic in ϕ . $G_{yx}(x > L)$ is exactly zero for the case $\mu_t = \mu_b$.

Turning to the dependence of the two conductances on b , in Fig. 2(e), we find monotonic dependence of G_{xx} on $|b|$ for $|\cos \phi|$ close to 1 and oscillatory dependence of G_{xx} on $|b|$ for $|\cos \phi|$ small compared to 1. This is because, the displacement of TI Dirac cones on in y direction is by an amount proportional to $\cos \phi$. Nearly normal incidences with θ close to zero contribute the most to G_{xx} . When $|\cos \phi|$ is large, for angles of incidences θ close to zero, the transport in TI region is diffusive characterized by a complex $k_{x,p,s}$ whose imaginary part grows in magnitude with b . When $|\cos \phi|$ is small compared to 1, the displacement of the TI Dirac cones along y -direction is minimal. Nearly normal incidences from NM will find a real $k_{x,p,s}$ in the TI and the transport is ballistic except for scatterings at the interfaces which leads to interference between the forward moving and the backward moving waves. This is the reason for oscillatory behavior of G_{xx} with b . Under the transformation $\phi \rightarrow \phi + \pi$, the transmission probabilities $|t_{\sigma,\sigma'}|^2$ for angles of incidence θ and $-\theta$ get interchanged thereby making G_{xx} even in b . The nonzero values of the transverse conductance G_{yx} at certain values of ϕ increases in magnitude with $|b|$ for small $|b|$ since increasing value of $|b|$ gives scope for higher asymmetry between scatterings at angles of incidence θ and $-\theta$. But beyond a value of $|b|$, the displacement of the Dirac cone in y -direction causes the wavefunction to decay into the TI (which is particularly the case for $|\cos \phi|$ close to 1), resulting in decrease in magnitude of G_{yx} with $|b|$. For values of ϕ such that $|\cos \phi|$ is small compared to 1, the scattering from angles of incidence away from normal incidence centered around

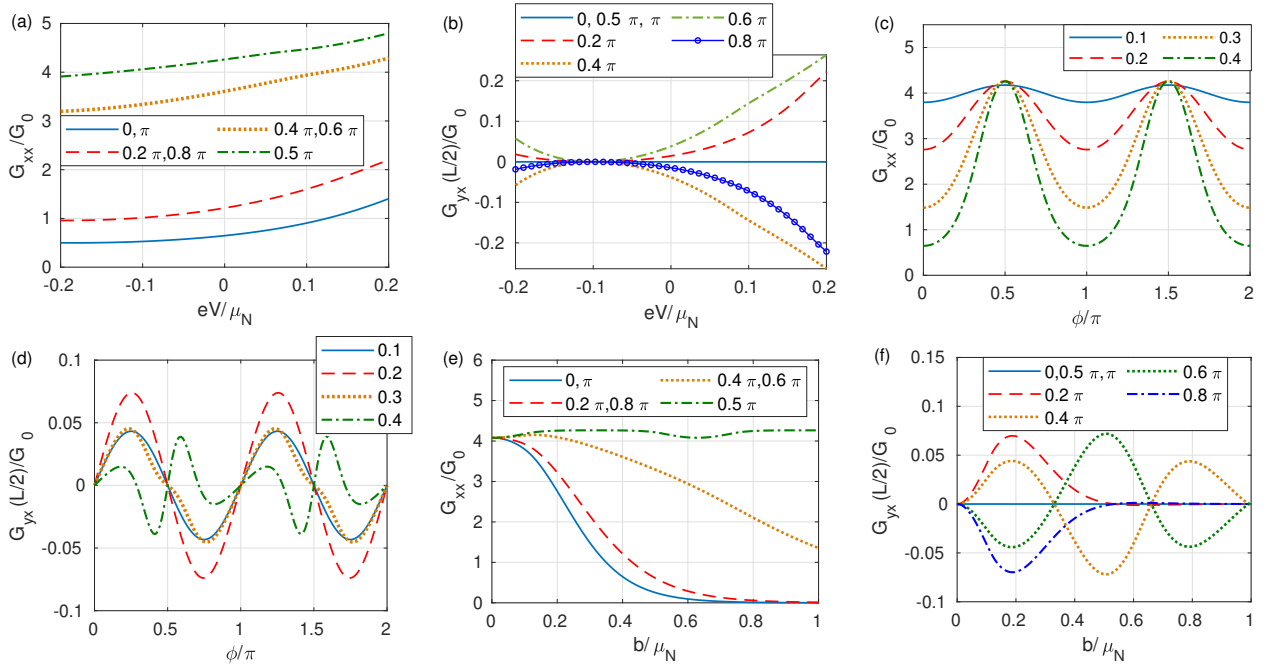


FIG. 2. (a) G_{xx} and (b) G_{yx} as functions of bias for different angles ϕ made by the in-plane magnetic field with x -axis with $b = 0.4\mu_N$. The values shown in the legend for (a) are the respective values of ϕ for which G_{xx} is plotted. (c) G_{xx} and (d) G_{yx} at zero bias as functions of ϕ at different values of magnetic field mentioned within the plot. (e) G_{xx} and (f) G_{yx} at zero bias as functions of magnetic field b for different ϕ specified in the plot legends. Parameters: $L = 5\hbar v_F/\mu_N$, $\mu_t = \mu_b = 0.1\mu_N$ and $m = 0.025\mu_N/v_F^2$.

$\pm\theta_b$ which depend on $|b|$ contribute dominantly to G_{yx} . The Fabry-Pérot type interference²¹ of these modes results in oscillations in G_{yx} with $|b|$. Under $\phi \rightarrow \phi + \pi$, the displacement of each of the Dirac cones is opposite to that before the transformation. This hints at the reversal of sign of G_{yx} upon $b \rightarrow -b$. But, since $b_y \rightarrow -b_y$ the displacement of each of the Dirac cones along x is opposite to that before the transformation making the surface dominantly contributing to G_{yx} switch under the transformation $\phi \rightarrow \phi + \pi$. Hence the displacement of the Dirac cone along y -direction for the surface dominantly contributing to G_{yx} is shifted in the same direction for both choices of magnetic field directions ϕ and $\phi + \pi$, making G_{yx} π -periodic. To study the dependence of the transverse conductance on the location, we plot $G_{yx}(x)$ versus x in Fig. 3. We find that the magnitude of the transverse conductance is peaked at $x = L/2$.

B. $\mu_t \neq \mu_b$

To study the conductances in this case, we choose the same set of parameters as in the Fig. 2 except when mentioned specifically. We choose $\mu_t = -\mu_b = 0.1\mu_N$. The longitudinal differential conductance shows characteristics very similar to the ones in Fig. 2(c) except for a change in the numerical value. In Fig. 4, we plot the transverse differential conductances at $x = L/2$ and at

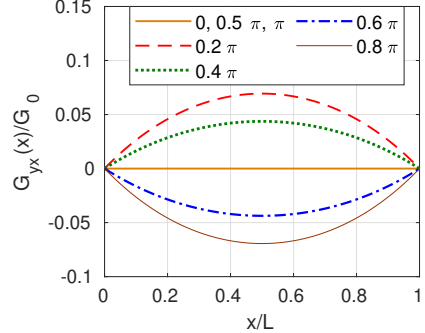


FIG. 3. Dependence of the transverse differential conductance on the location in the TI region for different angles ϕ mentioned in the legend with the choice of parameters: $L = 5\hbar v_F/\mu_N$, $\mu_t = \mu_b = 0.1\mu_N$ and $m = 0.025\mu_N/v_F^2$.

$x > L$ versus ϕ . It is interesting to see that $G_{yx}(x)$ is 2π -periodic for $\mu_t = -\mu_b$. Also, $G_{yx}(x > L)$ is nonzero generically except at zero bias for which it is always zero. Also, interestingly both $G_{yx}(L/2)$ and $G_{yx}(x > L)$ are nonzero at $\phi = 0$ for this case. This is because of the displacement of the two Dirac cones in $\pm y$ -direction equally but in opposite directions does not lead to cancellation of transverse currents at nonzero bias due to broken perfect antisymmetry. For a fixed bias, the values of $G_{yx}(x)$ for ϕ and $\pi - \phi$ are equal in magnitude and opposite in

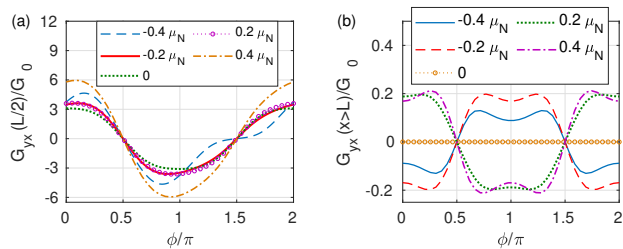


FIG. 4. Transverse differential conductance $G_{yx}(x)$ at (a) $x = L/2$ and at (b) $x > L/2$ as functions of ϕ for different values of bias mentioned in the legend. $\mu_t = -\mu_b = 0.1\mu_N$, $L = 5\hbar v_F/\mu_N$, and $m = 0.025\mu_N/v_F^2$.

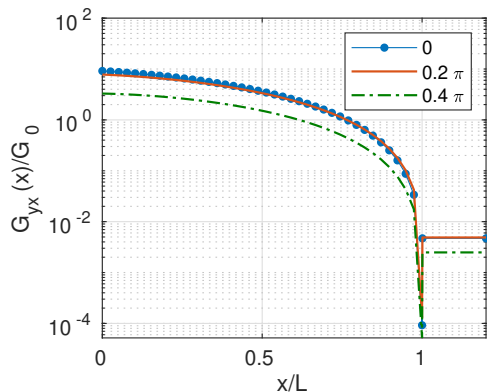


FIG. 5. Transverse conductance as a function of the location for different choices ϕ indicated in the legend. Parameters same as in Fig. 4 and bias $0.2\mu_N$.

sign. In Fig. 5, we plot $G_{yx}(x)$ versus x for the same choice of parameters as before, fixing the bias at $0.2\mu_N$ for different choices of ϕ .

IV. DISCUSSION AND CONCLUSION

We have essentially studied the phenomenon of PHE in TIs with the scattering theory approach when TI is connected to NM leads on either sides. We use the boundary condition for the NM-TI junction obtained by demanding the current conservation. The longitudinal and the transverse conductances are π -periodic in ϕ when $\mu_t = \mu_b$. When $\mu_t \neq \mu_b$, the longitudinal conductance is still π -periodic in ϕ whereas the transverse conductance becomes 2π -periodic in ϕ . For angles ϕ close to 0 or π , the longitudinal conductance decays with magnetic field whereas for angles ϕ close to $\pm\pi/2$, the longitudinal conductance decays with the magnetic field much slowly showing a slight periodic behavior with magnetic field at $\phi = \pm\pi/2$. Magnitude of the transverse conductance first increases with magnetic field, peaks and then decreases for angles ϕ close to but not equal to 0 or π whereas oscillates after an initial monotonic increase for angles close to $\pm\pi/2$. Such oscillations are rooted in Fabry-Pérot type interference in the TI region. The transverse conductance depends on the location and is maximum in magnitude exactly at the middle between the two TI-NM junctions and is zero in the right NM lead when $\mu_t = \mu_b$. When $\mu_t = -\mu_b$, the transverse conductance is maximum at the left NM-TI junction and is nonzero though small in magnitude in the right NM region. The differential gating of the top and the bottom surfaces of the TI can be experimentally achieved which means μ_t and μ_b can be separately controlled⁸. The angular dependence of the transverse resistance for the case of differentially gated top and bottom surfaces of the TI needs to be probed experimentally.

ACKNOWLEDGMENTS

Authors thank Bertrand Halperin, Karthik V. Raman and Archit Bhardwaj for useful discussions. AS thanks DST-INSPIRE Faculty Award (Faculty Reg. No. : IFA17-PH190) for financial support.

* Corresponding author: abhirams@uohyd.ac.in

- ¹ X.-L. Qi and S.-C. Zhang, "Topological insulators and superconductors," *Rev. Mod. Phys.* **83**, 1057–1110 (2011).
- ² M. Z. Hasan and C. L. Kane, "Colloquium: Topological insulators," *Rev. Mod. Phys.* **82**, 3045–3067 (2010).
- ³ B. Yan and C. Felser, "Topological materials: Weyl semimetals," *Annual Review of Condensed Matter Physics* **8**, 337–354 (2017).
- ⁴ N. P. Armitage, E. J. Mele, and A. Vishwanath, "Weyl and dirac semimetals in three-dimensional solids," *Rev. Mod. Phys.* **90**, 015001 (2018).
- ⁵ A. A. Burkov, "Giant planar hall effect in topological metals," *Phys. Rev. B* **96**, 041110 (2017).

- ⁶ S. Nandy, Girish Sharma, A. Taraphder, and S. Tewari, "Chiral anomaly as the origin of the planar hall effect in weyl semimetals," *Phys. Rev. Lett.* **119**, 176804 (2017).
- ⁷ N. Kumar, S. N. Guin, C. Felser, and C. Shekhar, "Planar hall effect in the weyl semimetal gdptbi," *Phys. Rev. B* **98**, 041103 (2018).
- ⁸ A. A. Taskin, H. F. Legg, F. Yang, S. Sasaki, Y. Kanai, K. Matsumoto, A. Rosch, and Y. Ando, "Planar hall effect from the surface of topological insulators," *Nat. Commun.* **8**, 1340 (2017).
- ⁹ D. Rakhmievich, F. Wang, W. Zhao, M. H. W. Chan, J. S. Moodera, C. Liu, and C.-Z. Chang, "Unconventional planar hall effect in exchange-coupled topological insulator-ferromagnetic insulator heterostructures," *Phys.*

- Rev. B **98**, 094404 (2018).
- ¹⁰ P. He, S. S.-L. Zhang, D. Zhu, S. Shi, O. G. Heinonen, G. Vignale, and H. Yang, “Nonlinear planar hall effect,” *Phys. Rev. Lett.* **123**, 016801 (2019).
 - ¹¹ S.-H. Zheng, H.-J. Duan, J.-K. Wang, J.-Y. Li, M.-X. Deng, and R.-Q. Wang, “Origin of planar hall effect on the surface of topological insulators: Tilt of dirac cone by an in-plane magnetic field,” *Phys. Rev. B* **101**, 041408 (2020).
 - ¹² S. Nandy, A. Taraphder, and S. Tewari, “Berry phase theory of planar hall effect in topological insulators,” *Scientific Reports* **8**, 14983 (2018).
 - ¹³ B. Scharf, A. Matos-Abiague, J. E. Han, E. M. Hankiewicz, and I. Žutić, “Tunneling planar hall effect in topological insulators: Spin valves and amplifiers,” *Phys. Rev. Lett.* **117**, 166806 (2016).
 - ¹⁴ R. Landauer, “Spatial variation of currents and fields due to localized scatterers in metallic conduction,” *IBM J. Res. Dev.* **1**, 223–231 (1957).
 - ¹⁵ M. Büttiker, Y. Imry, R. Landauer, and S. Pinhas, “Generalized many-channel conductance formula with application to small rings,” *Phys. Rev. B* **31**, 6207 (1985).
 - ¹⁶ S. Datta, *Electronic transport in mesoscopic systems* (Cambridge University Press, Cambridge, 1995).
 - ¹⁷ S. Modak, K. Sengupta, and D. Sen, “Spin injection into a metal from a topological insulator,” *Phys. Rev. B* **86**, 205114 (2012).
 - ¹⁸ A. Soori, O. Deb, K. Sengupta, and D. Sen, “Transport across a junction of topological insulators and a superconductor,” *Phys. Rev. B* **87**, 245435 (2013).
 - ¹⁹ A. Soori, “Scattering in quantum wires and junctions of quantum wires with edge states of quantum spin hall insulators,” arXiv: 2005.11557 (2020).
 - ²⁰ D. Sen and O. Deb, “Junction between surfaces of two topological insulators,” *Phys. Rev. B* **85**, 245402 (2012); “Erratum: Junction between surfaces of two topological insulators [phys. rev. b 85, 245402 (2012)],” **86**, 039902 (2012).
 - ²¹ A. Soori, S. Das, and S. Rao, “Magnetic-field-induced fabry-pérot resonances in helical edge states,” *Phys. Rev. B* **86**, 125312 (2012).